The Role of Large-Scale Atmospheric Circulation in the Relationship between Tropical Convection and Sea Surface Temperature

K.-M. LAU

Climate and Radiation Branch, Laboratory for Atmosphere, NASA/Goddard Space Flight Center, Greenbelt, Maryland

H.-T. WU

Applied Research Corporation, Landover, Maryland

S. BONY

Laboratoire de Meteórologie Dynamique, CNRS, Paris, France

(Manuscript received 13 November 1995, in final form 2 May 1996)

ABSTRACT

In this paper, the authors study the influence of the large-scale atmospheric circulation on the relationship between sea surface temperature (SST) and tropical convection inferred from outgoing longwave radiation (OLR). They find that under subsidence and clear sky conditions there is an increase in OLR with respect to SST at a rate of 1.8–2.5 Wm^{-2} $(°C)^{-1}$. In regions of large-scale ascending motions, which is correlated to, but not always collocated with, regions of warm water, there is a large reduction of OLR with respect to SST associated with increase in deep convection. The rate of OLR reduction is found to be a strong function of the large-scale motion field. The authors find an intrinsic OLR sensitivity to SST of approximately -4 to -5 Wm^{-2} $(°C)^{-1}$ in the SST range of 27°–28°C, under conditions of weak large-scale circulation. Under the influence of strong ascending motion, the rate can be increased to -15 to -20 Wm^{-2} $(°C)^{-1}$ for the same SST range. The above OLR–SST relationships are strongly dependent on geographic locations. On the other hand, deep convection and large-scale circulation exhibit a nearly linear relationship that is less dependent on SST and geographic locations.

The above results are supported by regression analyses. In addition, they find that on interannual timescales, the relationship between OLR and SST is dominated by the large-scale circulation and SST changes associated with the El Niño–Southern Oscillation. The relationship between anomalous convection and local SST is generally weak everywhere except in the equatorial central Pacific, where large-scale circulation and local SST appear to work together to produce the observed OLR–SST sensitivity. Over the equatorial central Pacific, approximately 45%–55% of the OLR variance can be explained by the large-scale circulation and 15%–20% by the local SST.

Their results also show that there is no fundamental microphysical or thermodynamical significance to the so-called SST threshold at approximately 27°C, except that it represents a transitional SST between clear-sky/subsiding and convective/ascending atmospheric conditions. Depending on the ambient large-scale motion associated with basin-scale SST distribution, this transitional SST can occur in a range from 25.5° to 28°C. Similarly, there is no magic to the 29.5°C SST, beyond which convection appears to decrease with SST. The authors find that under the influence of strong large-scale rising motion, convection does not decrease but increases monotonically with SST even at SST higher than 29.5°C. The reduction in convection is likely to be influenced by large-scale subsidence forced by nearby or remotely generated deep convection.

1. Introduction

Previous studies of the relationship between tropical convection and sea surface temperature (SST) have found that the frequency of occurrence of tropical convection increases dramatically at SST of $\sim$ 27°C to 28°C and that for SST $>$ 28°C, the relationship breaks down and convection is more strongly controlled by the large-scale moisture convergence (e.g., Gadgil et al. 1984; Graham and Barnett 1987; Gutzler and Wood 1990). Recently, Zhang (1993) has suggested that while other factors may come into play for SST $>$ 28°C, the increase in mean intensity of deep convection with SST is continuous with no abrupt change at any SST. Webster (1994) has argued that the increased deep convection for SST $>$ 28°C is a result of the large-scale motion arising from differential heating of the atmosphere between the warm pool and adjacent regions. Another peculiar feature in the observed convection–SST relationship is that deep convection tends to maximize at SST

Corresponding author address: Dr. William K.-M. Lau, Climate and Radiation Branch, Code 913, Laboratory for Atmosphere, NASA/Goddard Space Flight Center, Greenbelt, MD 20771.
E-mail: lau@climate.gsfc.nasa.gov

of approximately 29.5°C, beyond which convection appears to decrease with SST (Waliser and Graham 1993). Waliser (1995) has suggested that this may be related to the formation of localized hot spots with very high SST ($>$ 29.5°C) due to increased solar radiation in regions of strong subsidence forced by convection elsewhere. While some of the proposed mechanisms by previous authors have adequately addressed specific features in the observed outgoing longwave radiation (OLR)–SST relationship, the physical underpinnings for the full range of convection and SST variations remain somewhat enigmatic.

While large-scale circulation has often been invoked to account for the lack of one-to-one relationship between deep convection and SST for SST $>$ 28°C, there has not been any *quantitative* estimate of the role of the large-scale circulation in the convection–SST relationship over the entire SST range. More recent studies have pointed out the importance of quantifying the effect of large-scale dynamics versus local SST in considering climate feedback mechanisms associated with clouds and sea surface temperature (Fu et al. 1992; Hartmann and Michelsen 1993). In particular, Lau et al. (1994) have stressed that all processes contributing to a given relationship between two variables in nature are intertwined and occur simultaneously. Hence, a quantitative estimate of the effect of one specific variable on another while keeping all other variables unchanged—that is, partial derivatives—is difficult, if not impossible, to obtain. Strictly speaking, these partial derivatives can be obtained only from well-designed control numerical experiment using realistic general circulation models. For real systems, the best one can hope for is to develop methodologies that can be used to statistically isolate the controlling factors and estimate partial changes under conditons when these factors remain constant. This requires long-term (multiyear) data to provide sufficient sampling under different conditions. In this paper, we demonstrate that such methodologies can be developed to determine the relative roles contributed by the large-scale circulation and SST on the observed relationships between tropical convection and SST.

2. Data and analysis procedures

We use three datasets for this study: SST, OLR, and 200-mb wind divergence (DIV). The SST data are blended (satellite and in situ observations) analysis with a 2° lat × 2° long resolution from the Climate Analysis Center (Reynolds 1988). The OLR data, which will be used as a proxy for tropical convection, are from the Advanced Very High Resolution Radiometer (AVHRR) of NOAA operational polar orbiting satellites. The DIV data are derived from the European Centre for Medium-Range Weather Forecasts (ECMWF) analysis and are used as a measure of the dynamical state of the tropical atmosphere. All three datasets have been processed to provide monthly mean values on the same 5° lat × 5° long grid between 40°S and 40°N for the period from June 1985 through December 1989. All climatologies of SST, OLR, and DIV are computed for this period.

The analysis procedures are as follows. In section 3, we briefly present the conventional OLR–SST relationship to highlight some of its well-known but paradoxical characteristics. Then the OLR–SST relationship is stratified in terms of the underlying dynamical control (DIV). From these an ''intrinsic'' convection–SST relationship can be derived from conditions in which the circulation control is weakest. This method is also being used by Bony et al. (1997, manuscript submitted to *J. Climate*) for studying the effect of large-scale circulation on climate feedback mechanisms. In section 4, a regression analysis is carried out at every grid point between the OLR and DIV, and between SST and DIV to ''remove'' the influence of the large-scale circulation on OLR and SST, respectively. The residual fields denoted by OLRA and SSTA are then obtained by subtracting the regressed amount from the total fields. A correlation analysis is then applied to the residuals to obtain an estimate of OLR variability due to local SST influence. A similar regression analysis is also carried out for the OLR and DIV fields with and without the SST dependence so as to provide an estimate of the influence of SST on the OLR–DIV relationship. The results yielded by the above-mentioned complementary procedures are then compared and discussed in section 5. Concluding remarks are presented in section 6.

3. OLR–SST relationships

a. Basic features

In this section, we summarize some well-known basic features of the convection–SST relationship that are required to understand the main results of this paper. Figures 1a–c show the spatial distributions of the climatological means of SST, OLR, and DIV, respectively. From here on, we shall refer to OLR $<$ 240 Wm^{-2} as deep convection and OLR $>$ 250 Wm^{-2} as clear-sky condition in the sense of monthly mean and spatial averages over the size of the OLR grid box. Comparison of Figs. 1a and 1b reveals an obvious similarity between the spatial patterns of SST and OLR, with deep convection located over the warm pool (SST $>$ 28°C) of the western Pacific/eastern Indian Ocean and the extension of warm water tongue over the eastern Pacific intertropical convergence zone (ITCZ). A closer examination reveals some significant differences between the OLR and SST patterns. For example, within the Tropics, the spatial gradients of the convection patterns are much tighter and features are more well defined in OLR than in SST. Within the convective zone of the western Pacific, subcenters of deep convection are found anchored to the maritime continent of New Guinea, Borneo, and Sumatra. Such subcenters are not found in the SST field (Fig. 1a) but in the DIV field (Fig. 1c). We note that

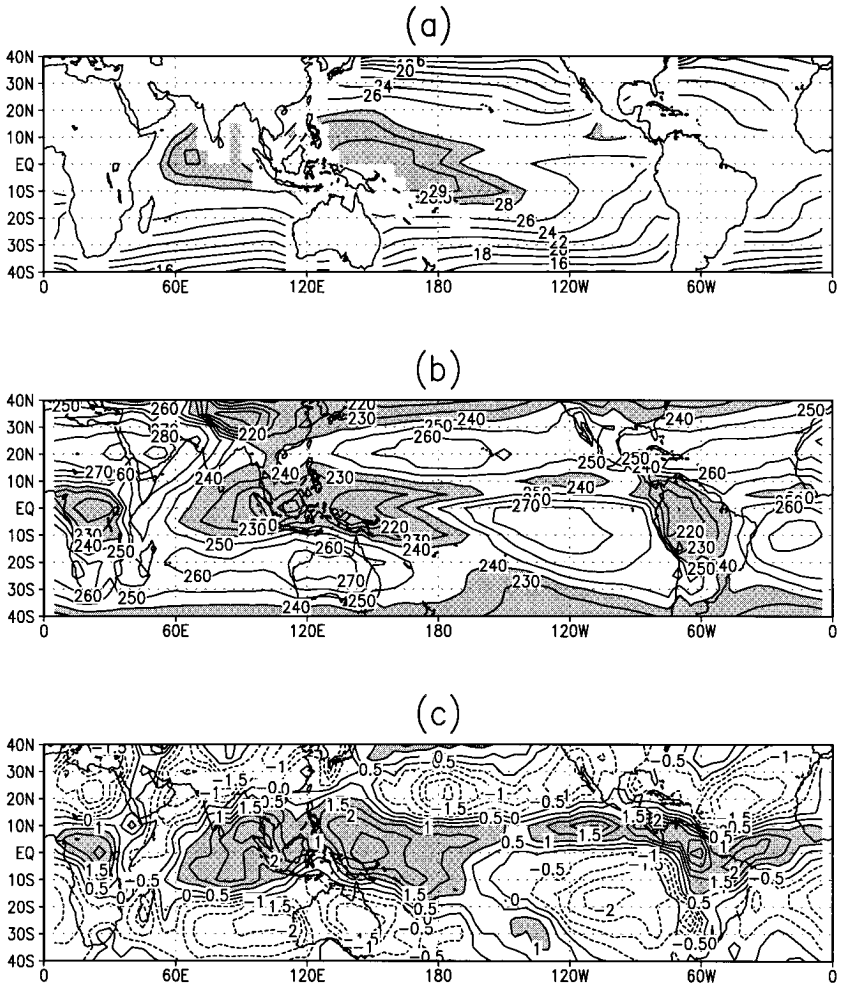

FIG. 1. Spatial distribution of the climatological annual means of (a) SST in °C, (b) OLR in Wm^{-2}, and (c) DIV in s^{-1}.

this may be due in part to the coarse resolution in the blended SST analysis used in this paper. A new SST analysis by Reynolds and Smith (1994) has indicated stronger gradient in SST than shown here. However, the analysis differences are not large enough to account for the different features noted here. Overall, the spatial distribution of DIV, including locations of the primary and secondary maxima, show better correspondence with OLR, compared to that of SST. Note that the regions of upper-level divergence (rising motion) and convergence (sinking motion) are closely tied to regions of deep convection and to regions with mean clear sky condition.

A commonly used representation of the relationship between OLR and SST is a scatterplot of colocated SST and OLR gridpoint values as shown in Fig. 2. The bulk OLR–SST relationship is represented by the solid line that connects the mean OLR values (represented by open circles) for every 0.5°C SST bin. This plot is comprised of a total of over 40 000 data points. Plots similar to Fig. 2 have been examined in great detail by many previous studies. The most conspicuous feature is the elbow-like pattern, marked by the rapid up-turn of the OLR–SST curve at about 27°–28°C. To facilitate subsequent discussions, we have identified the following SST–OLR regimes:

SST–OLR1: an increasing OLR with increasing SST from 18°C to 26°C,

SST–OLR2: a steep decrease in OLR with SST from 26.5°C to 29.5°C, and

SST–OLR3: a drop-off of OLR with increasing SST for SST $>$ 29.5°C.

Previous studies have demonstrated that the increase in OLR with SST in SST–OLR1 is primarily due to increasing SST minus the opposing effects of increasing water vapor under clear-sky conditions. The slope in this regime is approximately $+2.5$ $Wm^{-2}(°C)^{-1}$, in agreement with previous estimates of clear sky outgoing longwave radiation (e.g., Cess et al. 1990). From the scatter of the data points with OLR $<$ 240 Wm^{-2}, it is clear that deep convection, though not the modus operandi in the SST range of 18°–26°C, can still occur. In

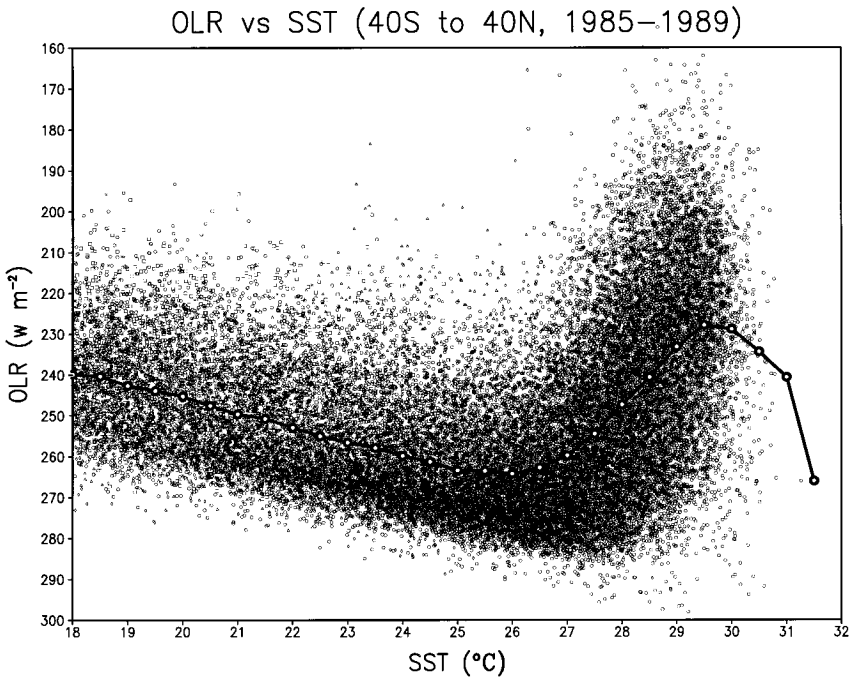

FIG. 2. Scatter diagram of collocated SST and OLR gridpoint values for the global tropical oceans (40°S–40°N). Superimposed is the mean OLR values as a function of every 0.5°C SST bin.

SST–OLR2, the steep rise in the OLR–SST relationship can be ascribed to the rapidly increasing occurrence of deep convection over warm water. The large scatter in the low OLR values signals the inherent temporal and spatial variabilities of deep convection, which are not matched by the SST variation, but may be related to the large-scale moisture convergence (Gadgil et al. 1984; Graham and Barnett 1987). The third regime, SST–OLR3, has been attributed to the presence of hot spots in isolated regions of forced subsidence within the western Pacific warm pool (Waliser 1995). From Fig. 2, we note that the statistics of SST–OLR3 at extreme high SSTs (>30.5°C) is contributed by relatively small number of data points outside the data envelope and therefore may be affected by sampling errors.

b. Classification of circulation regimes

To examine the SST–OLR relationship as a function of the large-scale motion, we divide the circulation regimes of the tropical atmosphere into seven categories according to the strength of the upper-level divergence. This classification is similar to that proposed by Bony et al. (1997, manuscript submitted to *J. Climate*), who used large-scale vertical motion to classify the different circulation regimes. The definition of the categories and the total number of data points in each category are shown in Table 1. Categories I through III represent upper-level divergence (ascending motion), Category IV weak divergence, and Category V through VII upper-level convergence (subsidence). Table 1 shows that within the domain from 40°S to 40°N, each circulation category is populated with more than three thousand data points, with category IV and V having the maximum population of around nine thousand points. For the tropical domain (20°S to 20°N), each of the circulation categories is well populated with at least two thousand data points. The large number of data points ensures that sufficient samples can be obtained from

TABLE 1. Classification of circulation regimes according to the strength of the upper-level divergence (DIV) and total number of data points in each category. Here, ∂OLR/∂SST denotes the partial rate of change of OLR w.r.t. SST at constant DIV for SST between 27°C to 28°C in unit of Wm^{-2} $(°C)^{-1}$.

DIV (10^{-6} s^{-1})	>2.5	[1.5, 2.5]	[0.5, 1.5]	[−0.5, 0.5]	[−1.5, −0.5]	[−2.5, −1.5]	<−2.5
Category	I	II	III	IV	V	VI	VII
# of data points							
(40°S–40°N)	3791	4407	7065	9401	8989	5347	3718
(20°S–20°N)	3169	3110	4956	4167	3907	2624	2122
∂OLR/∂SST	−15.2	−10.7	−9.0	−4.5	−3.1	−3.3	−6.2

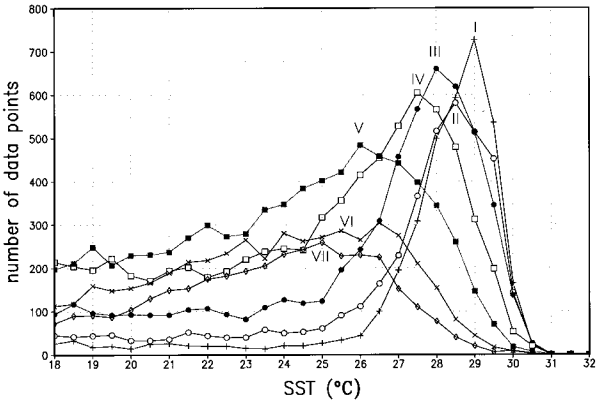

FIG. 3. Frequency distribution of SST, stratified according to seven DIV categories, with category I denoting strongest large-scale rising motion and category VII strongest subsidence motion (see Table 1 for definition of category).

each category and for different spatial domains to obtain statistically meaningful distributions.

Before discussing the circulation-stratified OLR–SST relationships, it is helpful to illustrate the frequency distribution of the SST as a function of the circulation regimes (Fig. 3). Two basic distribution patterns can be seen. First, all the SST frequency histograms for the ascent categories (I, II, and III) show sharply skewed distributions with SST concentrated at 28°C and higher. The sharp decline in population for SST $>$ 30°C is quite pronounced. Second, for the large-scale subsidence categories (V, VI, and VII), the SST distributions have much broader and less-defined peaks, and are heavily populated with SSTs less than 27°C. Of particular interest is category IV, which represents conditions of vanishing upper-level divergence. This category has maximum frequency of occurrence of SST between 27°C and 28°C and represents a transitional regime between the above-described basic distributions. The importance of this category will be discussed later.

The aforementioned classification also yields useful information regarding the geographical regions where the data points are sampled to obtain the OLR–SST relationship. Figure 4 shows the spatial distribution of the DIV categories in terms of the percentage occurrence of that category at each grid point. For brevity, only the distributions of categories I, VI, and VII are shown. The other categories can be inferred by interpolation between these categories. Category I (Fig. 4a) recaptures basic features of the warm pool of the western Pacific, the eastern Indian Ocean and the eastern Pacific ITCZ. Category VII (Fig. 4c) shows that the main contributions are from regions of frequent clear-sky or low cloud occurrences in the subtropics in the central North Pacific and North Atlantic and off the coast of western South America and Australia. The nondivergent category IV (Fig. 4b) pattern is not very well defined, having about equal (10%–20%) contributions from the large portions of the tropical and subtropical oceans. Examination of the spatial patterns for all categories reveals that the middle categories, III–V, which possess the least well-defined features, have a larger number of data points compared to those of the extreme categories, which have well-defined features. In particular, as noted above, category IV samples over a large portion of the tropical ocean under conditions in which the large-scale dynamical control is weakest. Therefore, category IV may provide an estimate of an intrinsic OLR–SST relationship when influence from the large-scale circulation is minimal, that is, this relationship should be closer to the true thermodynamical sensitivity of OLR due to local SST. We note that even in this category, the SST–OLR relationship will still be affected by dynamics in the form of local large-scale circulation convergence not resolved by the monthly mean. Since the OLR signal in the extratropics may not be representative of deep convection, we have computed the distributions for different latitude domains (20°S–20°N, 25°S–25°N, and 30°S–30°N). Except for the reduction of data points in the low-SST ($<$26°C) range, the above description remains essentially unchanged for all categories.

c. Circulation-stratified OLR–SST relationships

To avoid possible ambiguity regarding the representation of deep convection in the extratropics, the results of this section are derived from data points within the latitudinal domain 20°S–20°N (see Fig. 4). The OLR–SST relationships for the different DIV categories are shown in Fig. 5. The OLR–SST curves are obtained as in Fig. 2 by computing the mean of the OLR values at every 0.5°C SST bin. In addition, the standard errors of the mean, shown as error bars in Fig. 5, are also computed based on the data points within each SST bin. The variation of the OLR values within a given category and likewise the separation between different categories will be considered significant if the variation or the separations are much larger than the error bars. The ''clear-sky'' portions of the relationship in the SST–OLR1 regime, contributed mostly from the subsidence categories V through VII, all indicate a near-constant slope of about 1.8 $Wm^{-2}(°C)^{-1}$, which is significantly less than that ($=$2.5 $Wm^{-2}(°C)^{-1}$) estimated for the larger domain shown in Fig. 2. As discussed previously, this slope is related to the clear-sky infrared emission due to SST rise minus the effect of water vapor increase. From Fig. 4c, it can be seen that when the domain is restricted to 20°S–20°N, most of the data points are from the tropical eastern Pacific, with those from the subtropical subsidence zones greatly reduced. Thus this slope may be more representative of the clear-sky conditions under the subsidence branch of the Walker circulation over tropical eastern Pacific. As long as the clear sky/subsidence condition is maintained, the slope appears to be nearly independent of the large-scale circulation as evident in the asymptotic behavior of categories V–VII in the SST–OLR1 regime. This slope may represent a fun-

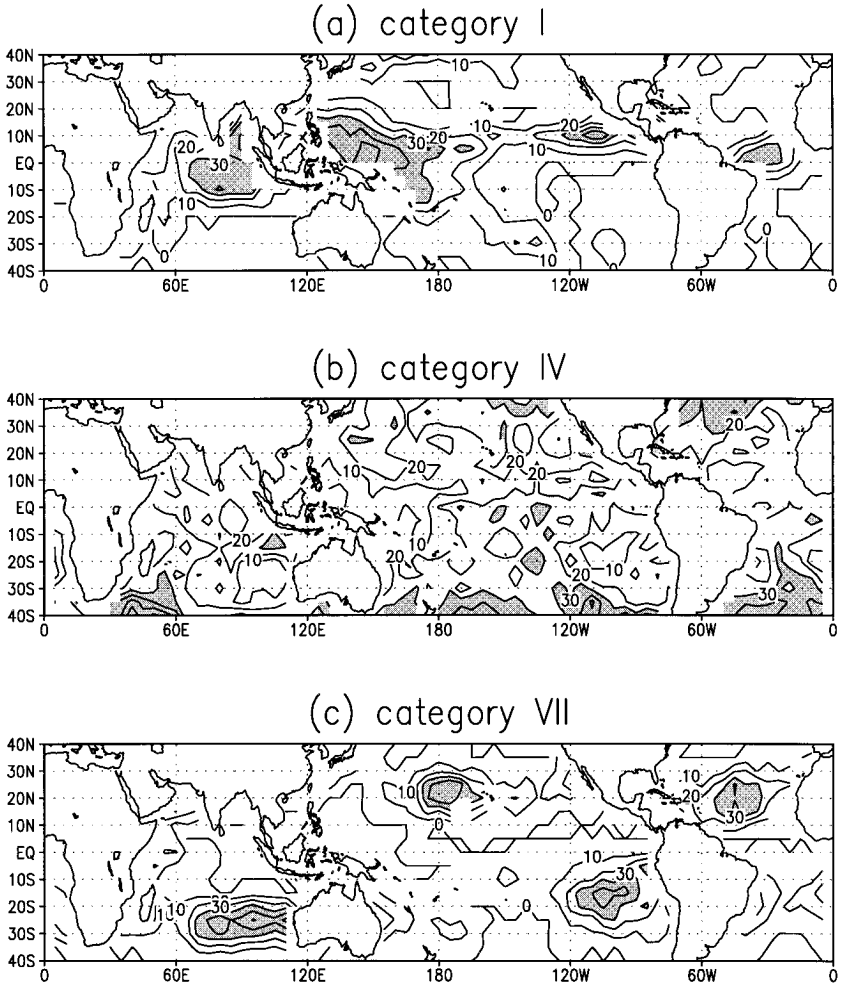

FIG. 4. Spatial distribution of the DIV (a) category I, (b) category IV, and (c) category VII in terms of the percentage occurrence at each grid point. Shaded areas indicate percentages exceeding 30%.

damental thermodynamic-radiation sensitivity to SST. It is obvious that the ascending categories I, II, and III contribute very little to the relationship in the SST–OLR1 regime.

In the SST–OLR2 regime, the OLR–SST relationships are well defined and well separated for each large-scale circulation category, except perhaps for category VII. In this regime, the influence of the large-scale motion is quite obvious. Here, while the increase in convection with SST can be found in all DIV categories, the decrease in OLR (increase in convection) is quite gradual with no obvious sharp SST thresholds. Most importantly, the rate of increase of convection (decrease of OLR) with respect to SST is substantially different for different DIV categories. For the ascending categories (I, II, and III), deep convection increases steeply with increasing SST. Much of the increase in convection is due to the increase in the large-scale ascending motion. Referring to Table 1, for category I,

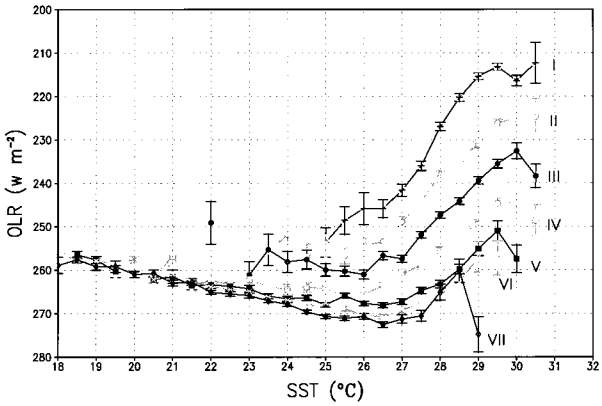

FIG. 5. Circulation-stratified OLR–SST relationship for the tropical domain (20°S–20°N) expressed as mean OLR values for every 0.5°C SST bin. Error bars indicate standard error of mean computed based on the total number of data points within each SST bin.

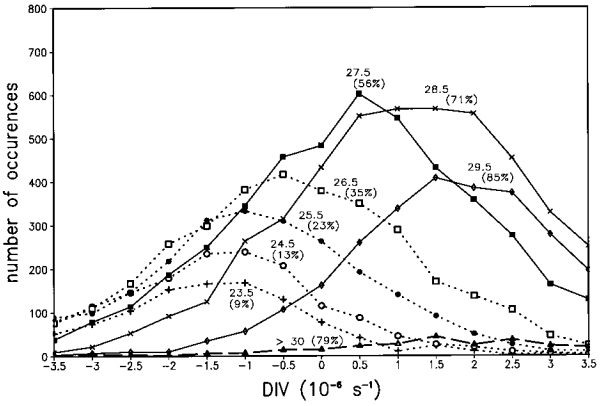

FIG. 6. Frequency distribution of DIV, stratified according to SST. Distributions for SST $<$ 27°C are shown as dotted lines and those between 27.5°C to 29.5°C as solid lines. The distribution for SST $>$ 30°C is shown by the thick dashed line. SST bin with 1°C interval is used. Also shown (in parentheses) is the fractional occurrence of data points with DIV $> 0.5 \times 10^{-6}$ s^{-1} for each SST category.

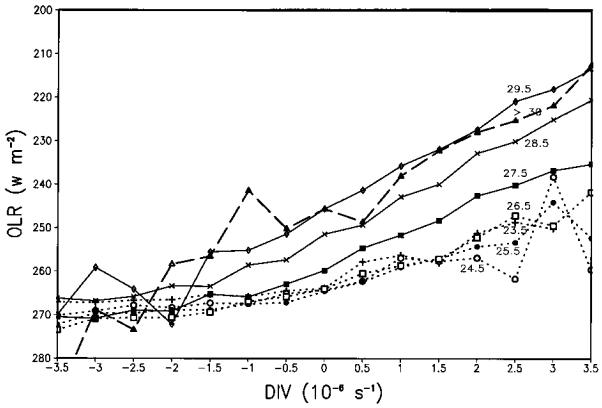

FIG. 7. OLR–DIV relationships as a function of SST, expressed as the mean OLR values for every 0.5×10^{-6} s^{-1} DIV bin, stratified according to the SST bins used in Fig. 6.

$$\frac{\partial(\mathrm{OLR})}{\partial(\mathrm{SST})}$$

at 27°–28°C is -15.2 Wm^{-2}(°C)$^{-1}$, much steeper than that for category IV, which only has a slope of -4.5 Wm^{-2}(°C)$^{-1}$. As pointed out earlier, the latter corresponds to situations when the large-scale dynamic control is at a minimum and may therefore represent a fundamental (controlled mainly by thermodynamic) rate of increase in deep convection with SST. The sensitivity of OLR to SST reduces further for the stronger subsidence categories (V and VI). The strongest subsidence category VII shows increased sensitivity of OLR to SST, but because of the smaller sample of SST $>$ 28°C for this category, this is almost certainly affected by sampling errors.

As for the SST–OLR3 regime, Fig. 5 shows that in the strong ascending region (categories I and II), the increase in deep convection with SST is monotonic with no significant decrease beyond 29.5°C. With the increasing influence of upper-level convergence (categories III through VII), a reversal in OLR–SST gradient begins to occur for higher SST. However, the turning point does not necessarily occur at 29.5°C. In general, there is a tendency for the OLR peak to occur at lower SST for increasing subsidence categories. For category III, the peak convection appears to occur at 30°C. For category V, it shifts to 29.5°C. For category VII, it appears to occur at 28.5°C, but with greater uncertainty. The gradient reversal is significant for categories III through V because of the relatively large sampling sizes (over several hundred to a thousand data points for each category as shown in Table 1) and the large separation among the mean of the different categories compared to its standard errors of the mean. For the strong subsidence categories (VI and VII), which are concentrated in the tropical eastern Pacific, the occurrence of relatively higher SSTs ($>$29.5°C) is extremely rare and the existence of a SST–OLR3 regime is questionable.

Further insight into the above OLR–SST relationships can be obtained by examining the OLR–DIV relationships as a function of SST. In particular, we like to point out that DIV itself is also dependent on the SST distribution being strongly driven by the SST gradient. Figure 6 shows the histogram of a total number of data points with respect to DIV, but stratified according to SST. In addition, the figure also shows the fractional occurrence of data point with DIV $> 0.5 \times 10^{-6}$ s^{-1} for each SST category. It can be seen that there is a progressively increasing proportion of rising motions (positive DIV) for SST from 23° through 29°C. Between the SST bins centered at 26.5°C and 27.5°C, there is a dramatic increase in the proportion of ascending motions from 35% to 56%. The proportion of ascending motion steadily increases with increasing SST (56% for 27.5°C to 85% for 29.5°C) until SST reaches the 29°–30°C range. For SST $>$ 30°C, the proportion of rising motion starts to decrease from 85% to 79%, that is, there is increasing subsidence motion at extreme high SST. Since high SST cannot physically cause the reduction of local convection, it may be argued that the reduced convection over extreme high SST is all remotely induced.

Unlike the OLR–SST relationship, the relationship between OLR and DIV appears to be quite linear for all categories. For SST $>$ 27°C, the slopes of the OLR–DIV curves are about 10–12 Wm^{-2} per unit change (10^{-6} s^{-1}) in the region of positive DIV. For low SST ($<$27°C), the slopes are about 4–5 Wm^{-2} per unit change in DIV and are nearly independent of the SST. Most of the sensitivity appears to come from the positive but not the negative DIV range. These sensitivities are consistent with the separation among the family of circulation-stratified OLR–SST relationships shown in Fig. 5. The above OLR–DIV relationship has been confirmed in a number of computations over different spatial and temporal domains and for a variety of seasonal and in-

terannual changes (not shown). These results suggest a fundamental coupling between OLR and DIV that is somewhat independent of SST.

4. Regression analysis

As illustrated above, the OLR–SST relationship shown in Fig. 2 is composed of a diverse mix of relationships that are strongly controlled by the large-scale circulation. As such, the relationship is difficult to interpret physically. The analyses in the previous section demonstrate that restricting the spatial domain to the Tropics can sharpen that relationship. Stratifying with respect to the large-scale circulation can unravel the relationship for better physical interpretations. In this section, we present results of a complementary methodology to those used in previous sections for understanding OLR–SST relationship for climate variability studies.

a. OLRA–SSTA relationships

To estimate the OLRA–SSTA (sea surface temperature anomaly) relationship for interannual climate variability, a linear regression analysis has been carried out, respectively, for OLR and SST versus DIV for all grid points in the tropical Pacific and Indian Oceans. The residuals (OLRA, SSTA) are then obtained by subtracting the linear dependence of OLR and SST on DIV from the total fields. These residuals will represent the would be anomalous OLR and SST, if the large-scale circulation were not operative. Obviously, the above procedure is imperfect as much as it is imprecise, because it is impossible in practice to separate the effect of atmospheric circulation from that due to local SST in the real world when both effects are operating and interacting simultaneously. However, by examining the linear dependence of OLR on SST and on DIV (see next section), we may be able to gain some additional insight into the mechanism responsible for the organization of tropical convection. We shall show that regression analyses yield results that are consistent with the categorization procedure discussed in the previous sections.

Figures 8a and b show the scatterplots of OLR versus SST at co-located grid points, across the equatorial Pacific before and after the large-scale divergence has been removed. It is obvious that in the total fields shown in Fig. 8a, the characteristic elbow feature consists of contributions from three different parts of the ocean basin, that is, the eastern, central, and western Pacific. Viewed alone, each region provides a very different type of SST–OLR relationship. There the OLR–SST relationship does not necessarily govern the way local tropical convection would behave if the underlying SST were raised from, say 22°C to 29°C. When the dependence on the atmospheric divergence is removed, the apparent relationship in the Fig. 8a plot is reduced to a cluster of points around the mean climate. Some weak relationships between OLRA and SSTA as a whole within the different regions can still be discerned, but the characteristic features are no longer present.

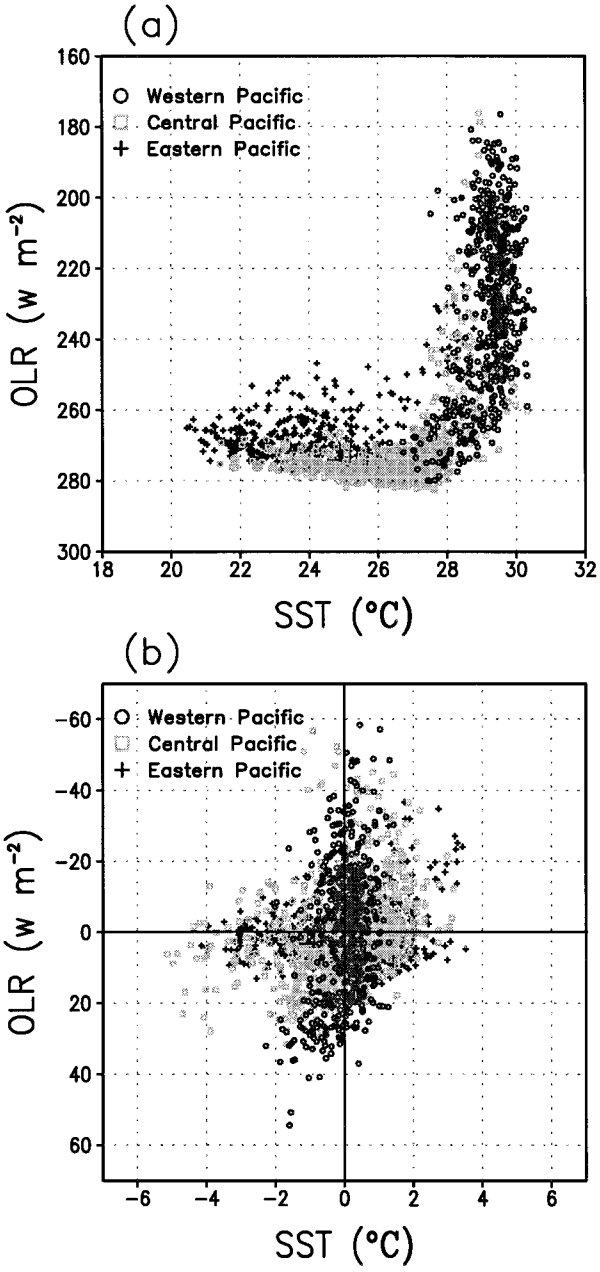

FIG. 8. Scatter diagram of OLR vs SST along equator for western Pacific (120°E to 175°E), central Pacific (180° to 125°W), and eastern Pacific (120°W to 180°W) (a) before and (b) after the linear dependence on DIV and the climatological mean values are removed.

Next, we examine the spatial dependence of the nonseasonal (annual cycle removed) OLR–SST relationship and estimate the relative contribution from the large–scale circulation. Figures 9a and b show the spatial distribution of the linear regression coefficients between convection and SST, at all the SST points, before and

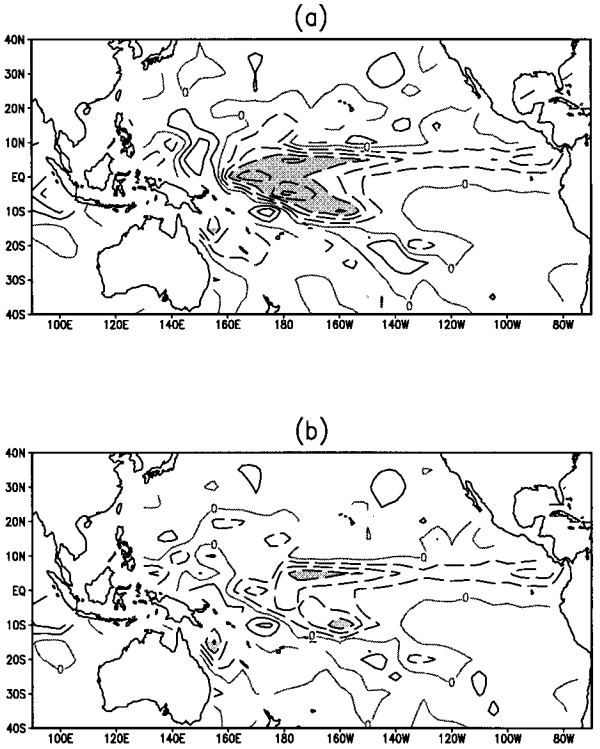

FIG. 9. Spatial distribution of linear regression coefficients between colocated OLR and SST (a) before and (b) after the linear dependence on DIV is removed. Contour interval is 5 $Wm^{-2}(°C)^{-1}$; negative contours are dashed; regions with values < -15 Wm^{-2} $(°C)^{-1}$ are shaded.

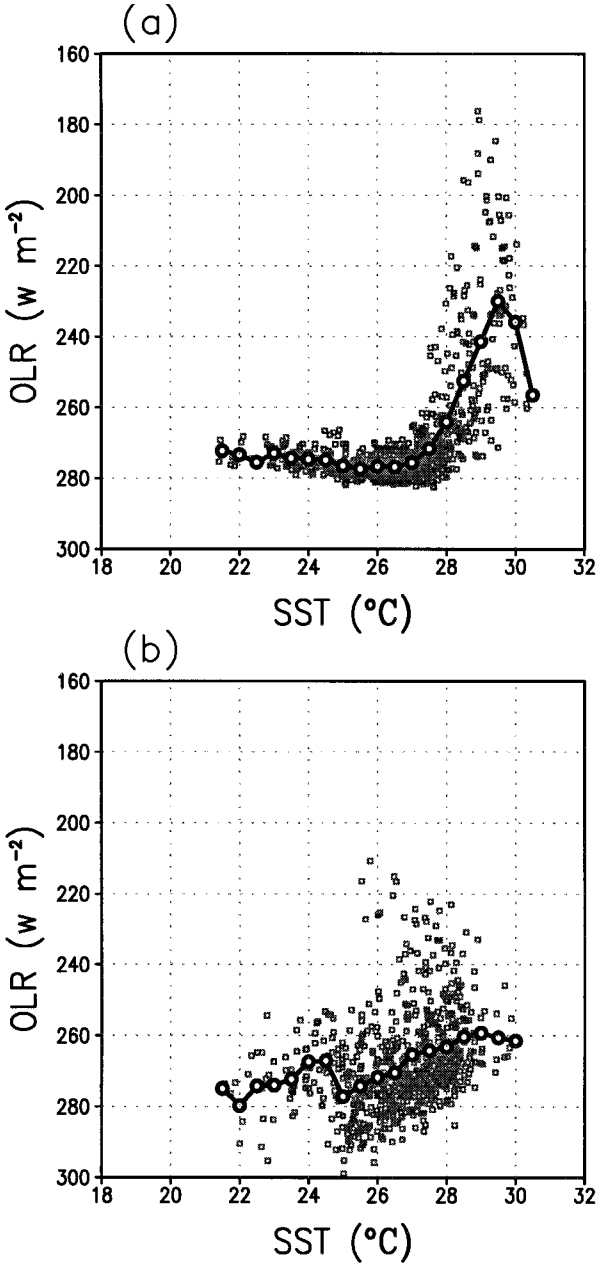

FIG. 10. OLR–SST scatterplot for the central equatorial Pacific (180° to 125°W) with mean OLR values for every 0.5°C SST bin superimposed (a) before and (b) after the linear dependence on DIV is removed.

after the large-scale circulation effect has been taken out, that is, (OLR–SST) versus (OLRA–SSTA). For OLR–SST (Fig. 9a), the pattern is reminiscent of the El Niño/Southern Oscillation (ENSO; e.g., Rasmusson and Wallace 1983) with largest SST sensitivity showing increased convection associated with increased local SST near the central part equatorial Pacific (indicated by the shaded region with absolute values higher than -15 $Wm^{-2}(°C)^{-1}$) where the maximum sensitivity is approximately -25 $Wm^{-2}(°C)^{-1}$. Over some areas of the western Pacific, the regression is weakly positive, indicating an apparent reduced convection with increasing SST. When the effect of the large-scale circulation is removed (Fig. 9b), the pattern remains essentially unchanged, but the sensitivity of OLRA to SSTA is reduced by 30%–70% everywhere. Over the central Pacific domain (160°E–160°W, 10°S–10°N), the average sensitivity is reduced to a range of -5 to -10 $Wm^{-2}(°C)^{-1}$. Here, the average correlation between OLR and SST is approximately -0.51. After the DIV effect is removed, the correlation is reduced to -0.35.

The above-noted reduced sensitivity of OLR to SST due to the removal of the effect of the large-scale circulation is consistent with that obtained from the OLR–SST relationship for Category IV (zero divergence). This is also evident in the OLR-SST scattered plots shown in Figs. 10a and 10b over the equatorial central Pacific before and after DIV is taken out. Here we restore the climatological mean fields to obtain a OLR–SST relationship similar to those shown in Figs. 2 and 5. As a result of the removal of the effect of DIV, the OLR sensitivity to local SST in the convective regime (corresponding to SST–OLR2 regime) is reduced significantly from about -20 $Wm^{-2}(°C)^{-1}$ (Fig. 10a) for SST in the range of 27°–29°C to approximately -4 to -5 $Wm^{-2}(°C)^{-1}$ (Fig. 10b) in the same range. Moreover,

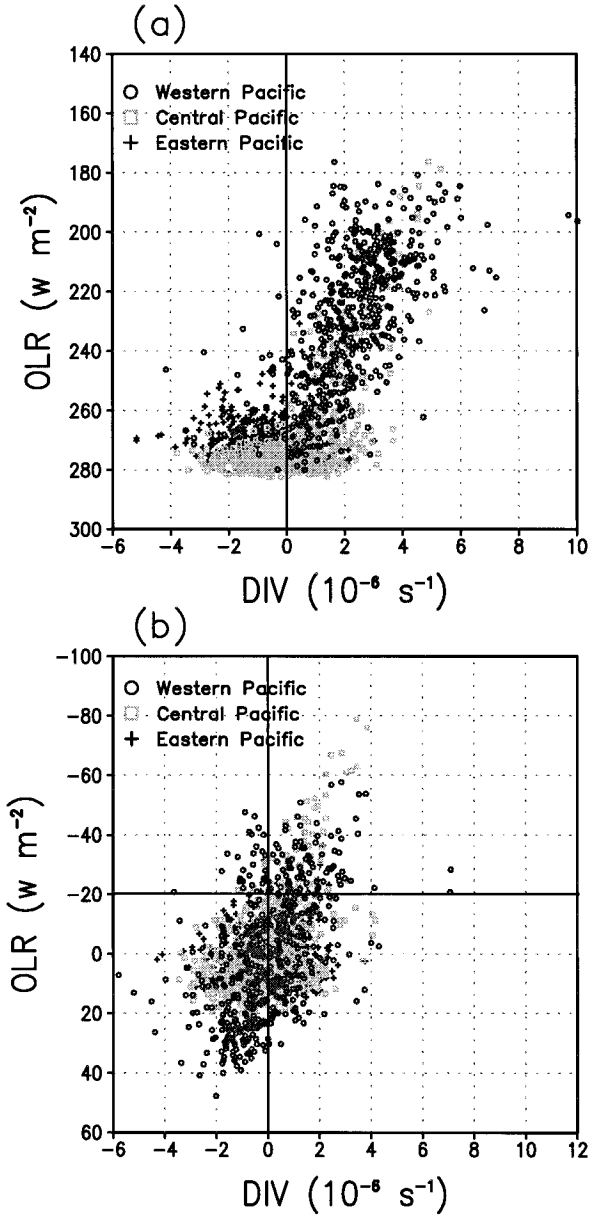

FIG. 11. Same as in Fig. 8 except for the scatterplot of OLR vs DIV for (a) before and (b) after the linear dependence on SST and the climatological mean values are removed.

the removal of DIV causes the apparent downturn of the SST–OLR curve in the high SST range (Fig. 10a) to disappear completely (Fig. 10b). This further supports the previous result that the observed maximum convection at 29.5°C in the bulk OLR–SST relationship (shown in Fig. 2) arises as a result of large-scale subsidence rather than from thermodynamical properties of water vapor versus temperature.

b. OLRA–DIVA relationships

In this subsection, we present results of a comparative analysis by ''removing'' the SST dependence of OLR and DIV using the same regression procedure as before. In this way, we allow the SST a ''first crack'' at explaining the fractional variance of OLR and OLR–DIV relationship. Figures 11a and b show the scatterplots of OLR versus DIV before and after the dependence of SST is removed, for the same domains as defined in Fig. 8. In the scatterplot for the total fields (Fig. 11a), there appears to be a linear relationship between OLR and DIV, indicating enhanced convection in the region of positive DIV. In the region of negative DIV, the relationship is not as clear. These are consistent with the features noted in Fig. 7. However, unlike those shown in Fig. 8, there is no obvious separation among different geographic regions in contributing to the basic linear relationship between OLR and DIV. The OLR–DIV relationship suggests a fundamental link between the large-scale circulation and tropical convection that is less dependent on the spatial domains compared to the OLR–SST relationship shown in Fig. 8. Figure 11b shows that the relationship between OLRA and DIVA remains quite similar to that before the SST dependence is removed. Over central Pacific domain, the correlation between OLR and DIV is -0.66 and -0.59 before and after the SST effect is removed. This reduction is considerably smaller than that caused by the removal of DIV from OLR (see discussion in the preceding subsection).

For more quantitative comparison, Tables 2a and 2b show the sensitivity of OLR to SST and DIV (in terms of regression coefficients), respectively, before and after removal of the influence of the third variable over the central Pacific domain. Also shown are the percentage of OLR variance explained either by SST or DIV. For comparison, similar regression coefficients and variances (shown in the last two columns of Table 2a and 2b) have also been computed for the nonseasonal fields, where the climatological seasonal cycle at each grid point is first removed. Table 2a shows that, averaged over the central Pacific domain, the sensitivity of OLR to SST is reduced substantially (from 15.3 to 8.3 $\mathrm{Wm}^{-2}(^{\circ}\mathrm{C})^{-1}$). For the total fields, the percentage reduction of sensitivity and fractional variance is 46% and 54%, respectively. These relative changes appear to hold also for the nonseasonal fields. As a comparison, from the bottom row of Table 2b, the reduction of the sensitivity of OLR to DIV and OLR fractional variance that is attributed to SST are only about 18% and 20%, respectively. For the nonseasonal fields, the corresponding percentage reductions are 19% and 16%. These percentages are considerably less than that shown in Table 1a both for the seasonal and the nonseasonal fields. Moreover, the fractional OLR variance explained by the DIV (columns two and four in Table 2b) are always larger than those explained by SST (columns two and four in Table 2a). These results again suggest that the DIV field may have relatively stronger control on the OLR variability and the OLR–SST relationship than

TABLE 2a. Sensitivity of OLR to SST over the central Pacific domain (160°E–160°W, 10°S–10°N), represented by the absolute value of the regression coefficients and fractional OLR variance explained by SST. Values for the DIV and no-DIV cases are shown separately. Results for the total fields are shown in the first two columns. The anomaly fields (with seasonal cycle removed) are shown in the last two columns.

	$\lvert\delta OLR/\delta SST\rvert$ [Wm^{-2} $°C)^{-1}$]	Fractional variance (r^2)	$\lvert\delta OLRA/\delta SSTA\rvert$ [$(Wm^{-2}$ $(°C)^{-1}$]	Fractional variance (r^2)
DIV	15.3	26%	10.4	13%
No DIV	8.3	12%	5.3	6%
% change	−46%	−54%	−49%	−54%

TABLE 2b. Same as in Table 2a except for sensitivity of OLR to DIV and the OLR fractional variance explained by DIV.

	$\delta OLR/\delta DIV$ [$(Wm^{-2}$ $(10^{-6}\,s^{-1})^{-1}$]	Fractional variance (r^2)	$\lvert\delta OLRA/\delta DIVA\rvert$ [$(Wm^{-2}$ $(10^{-6}\,s^{-1})^{-1}$]	Fractional variance (r^2)
SST	8.4	44%	7.5	38%
No SST	6.9	35%	6.1	32%
% change	−18%	−20%	−19%	−16%

SST on OLR variation and the corresponding OLR–DIV relationship.

5. Summary and discussion

In this section, we discuss some possible physical mechanisms that may shed light on the above results. It is obvious that different regimes of the OLR–SST relationships arise from the interplay of different mechanisms at work. The transitions between different regimes occur continuously and are controlled by both changes in SST distribution and the large-scale circulation. It is argued that there is no fundamental microphysical or thermodynamical importance to the so-called SST threshold for convection, except that it represents a SST range that separates the clear-sky/subsiding and deep convection/ascending conditions, which are controlled by the entire large-scale circulation/SST coupled system. Depending on the strength of the large-scale upward motion, the transition occurs at SST range of 25.5°C to 27.5°C. Below this range, the outgoing longwave radiation has a sensitivity of 1.8–2.5 $Wm^{-2}(°C)^{-1}$, consistent with that of clear-sky estimates from previous studies (e.g., Cess et al. 1990). For SST above this range, there is a large apparent decrease in OLR with SST. Much of the net decrease in OLR can be attributed to the increased occurrence of deep convection/high clouds overshadowing the background radiation. In this regime, the sensitivity of convection to local SST is strongly enhanced by the rising motions associated with the large-scale circulation. An intrinsic OLR–SST relationship, which is identified under conditions of weak to vanishing divergent motions, is found to have a moderate OLR sensitivity to SST of approximately $-5\ Wm^{-2}(°C)^{-1}$. Strong large-scale upward motion can enhance this sensitivity by more than threefold to about $-15\ Wm^{-2}(°C)^{-1}$.

Likewise, the presence of an apparent convection maximum (OLR minimum) at SST of about 29.5°C does not necessarily reflect a fundamental thermodynamic relationship between water vapor and temperature. In regions with strong ascending large-scale motion, convection increases monotonically with SST in the range of 26°–29°C and levels off beyond 29.5°C. The convection maximum occurs only in circulation regimes that have significant proportion of subsidence motions. A possible physical explanation of this behavior is that increased subsidence induced from neighboring and/or remote convection provides warming and drying of the atmosphere above the boundary layer through adiabatic processes, thereby producing temperature inversion that limits the formation of deep convection. The resulting increased occurrence of clear-sky conditions will allow more insolation to reach and lead to the extreme observed SST. In the western Pacific, these conditions may occur due to the seasonal shift of the ITCZ and the low-frequency variability such as the Madden–Julian Oscillation (e.g., Lau and Chan 1988). This is also consistent with the formation of ''hot spots'' in the warm pool of the western Pacific/Indian Ocean reported by Waliser (1995). In the tropical eastern Pacific, the competition is between the insolation that warms the ocean and the vigorous oceanic dynamics that cools it by upwelling. The presence of strong cold upwelling in the eastern Pacific ocean may be the reason why SST $>$ 28°C are seldom found, and ''hot spots'' are never detected over this region, except possibly during ENSO.

For interannual climate variations, we find that the ENSO signals dominate the SST–OLR relationships. The regions of highest OLR sensitivity to SST are found over the equatorial central Pacific, in agreement with the findings of Liu et al. (1994). During ENSO, it is well known that changes in the large-scale circulation are associated with the eastward migration of convection from the western Pacific to the central and eastern Pacific. The migration in convection is responsive to changes in the entire ocean–atmosphere circulation structure and, in particular, to the changes in the SST gradient (Lindzen and Nigam 1987). In the central Pacific, where the local correlation of SST to OLR is largest, we estimate that approximately 26% of the OLR variance is due to SST and 44% due to DIV. In this region, about 40%–50% of the apparent sensitivity of OLR to SST can be ascribed to the effect of the large-scale circulation. Our results suggest that the large-scale circulation may have relatively stronger control than local SST on OLR variance and sensitivites on monthly to interannual timescales.

6. Concluding remarks

It should be pointed out that the two separate approaches used in this paper, that is, categorization and regression analysis, both yield an estimate of the intrinsic (in the sense of free from the influence of large-scale circulation) OLR–SST sensitivity of -4 to -5 $\mathrm{Wm}^{-2}(^{\circ}\mathrm{C})^{-1}$, considerably weaker than the bulk sensitivity of -15 to -20 $\mathrm{Wm}^{-2}(^{\circ}\mathrm{C})^{-1}$ found in previous studies (e.g., Zhang 1993). The latter is presumably due to the juxtaposition of different circulation and SST regimes of diverse spatial and temporal scales. We also note that while the lower sensitivity in the intrinsic OLR–SST relationships found here may better reflect the underlying thermodynamical control, that is, that arising from the Clausius–Clapyeron relationship governing water vapor and convection by temperature change, the effect of large-scale circulation feedback on shorter timescales unresolvable by monthly averages is still present in the intrinsic relationship found here. Hence the underlying thermodynamical sensitivity of OLR to SST may be even weaker. It is important to note that in reality, there is a three-way coupling among the three variables, SST, OLR, and DIV, and it is impossible to isolate unambiguously, from the total fields, the mutual influence of any two variables when they are decoupled from the third. As such, the present analysis will not yield definitive results. Nonetheless, it will provide some clues as to the relative importance of one control versus the other and in unraveling the mechanisms of coupling between SST and atmospheric hydrologic processes. Clearly, the results and interpretation of the present study need further validation with more data and should be tested with numerical models.

REFERENCES

Cess, R. D., and Coauthors, 1990: Intercomparison and interpretation of climate feedback processes in 19 atmospheric general circulation models. *J. Geophys. Res.,* **95,**(D10) 16 601–16 615.

Fu, R., A. D. Del Genio, W. B. Rossow, and W. T. Liu, 1992: Cirrus-cloud thermostat for tropical sea surface temperature tested using satellite data. *Nature,* **358,** 394–397.

Gadgil, S., P. V. Joseph, and N. V. Joshi, 1984: Ocean–atmospheric coupling over monsoon regions. *Nature,* **312,** 141–143.

Graham, N., and T. P. Barnett, 1987: Sea surface temperature, surface wind divergence, and convection over tropical oceans. *Science,* **238,** 657–659.

Gutzler, D. S., and T. M. Wood, 1990: Structure of large-scale convective anomalies over the tropical oceans. *J. Climate,* **3,** 483–496.

Hartmann, D. L., and M. L. Michelsen, 1993: Large-scale effects on the regulation of tropical sea surface temperature. *J. Climate,* **6,** 2049–2062.

Lau, K.-M., and P. H. Chan, 1988: Intraseasonal and interannual variations of tropical convection: A possible link between the 40–50 day oscillation and ENSO? *J. Atmos. Sci.,* **45,** 506–521.

——, C. H. Sui, M. D. Chou, and W. K. Tao, 1994: An inquiry into the cirrus cloud thermostat effect for tropical sea surface temperature. *Geophys. Res. Lett.,* **21,** 1157–1160.

Lindzen, R., and S. Nigam, 1987: On the role of sea surface temperature gradient in forcing low-level winds and convergence in the Tropics. *J. Atmos. Sci.,* **44,** 2418–2431.

Liu, W. T., A. Zhang, and J. K. B. Bishop, 1994: Evaporation and solar irradiance as regulators of sea surface temperature in annual and interannual changes. *J. Geophys. Res.,* **99,** 12 623–12 637.

Rasmusson, E. M., and J. M. Wallace, 1983: Meteorological aspects of the El Niño/Southern Oscillation. *Science,* **222,** 1195–1202.

Reynolds, R., 1988: A real time global sea surface temperature analysis. *J. Climate,* **1,** 75–86.

——, and T. M. Smith, 1994: Improved global sea surface temperature analysis using optimum interpolation. *J. Climate,* **7,** 929–948.

Waliser, D. E., 1996: Formation and limiting mechanisms for very high sea surface temperature: Linking the dynamics and thermodynamics. *J. Climate,* **9,** 161–188.

——, and N. E. Graham, 1993: Convective cloud systems and warm pool sea surface temperatures: Coupled interactions and self-regulation. *J. Geophys. Res.,* **98,** 12 881–12 893.

Webster, P. J., 1994: Role of hydrological processes in ocean–atmosphere interactions. *Rev. Geophys.,* **32,** 427–476.

Zhang, C., 1993: Large-scale variability of atmospheric deep convection in relation to sea surface temperature in the Tropics. *J. Climate,* **6,** 1898–1912.